Cell

Complementary Sequence-Mediated Exon Circularization

Xiao-Ou Zhang,[1,4] Hai-Bin Wang,[2,3,4] Yang Zhang,[2] Xuhua Lu,[3] Ling-Ling Chen,[2,*] and Li Yang[1,*]
[1]Key Laboratory of Computational Biology, CAS-MPG Partner Institute for Computational Biology, Shanghai Institutes for Biological Sciences, Chinese Academy of Sciences, Shanghai 200031, China
[2]State Key Laboratory of Molecular Biology, Shanghai Key Laboratory of Molecular Andrology, Institute of Biochemistry and Cell Biology, Shanghai Institutes for Biological Sciences, Chinese Academy of Sciences, Shanghai 200031, China
[3]Department of Orthopedic Surgery, Changzheng Hospital, Second Military Medical University, Shanghai 200003, China
[4]Co-first authors
*Correspondence: linglingchen@sibcb.ac.cn (L.-L.C.), liyang@picb.ac.cn (L.Y.)
http://dx.doi.org/10.1016/j.cell.2014.09.001

SUMMARY

Exon circularization has been identified from many loci in mammals, but the detailed mechanism of its biogenesis has remained elusive. By using genome-wide approaches and circular RNA recapitulation, we demonstrate that exon circularization is dependent on flanking intronic complementary sequences. Such sequences and their distribution exhibit rapid evolutionary changes, showing that exon circularization is evolutionarily dynamic. Strikingly, exon circularization efficiency can be regulated by competition between RNA pairing across flanking introns or within individual introns. Importantly, alternative formation of inverted repeated *Alu* pairs and the competition between them can lead to alternative circularization, resulting in multiple circular RNA transcripts produced from a single gene. Collectively, exon circularization mediated by complementary sequences in human introns and the potential to generate alternative circularization products extend the complexity of mammalian posttranscriptional regulation.

INTRODUCTION

Covalently closed circular RNA molecules were originally found to naturally exist in plant viroids (Sanger et al., 1976) and hepatitis δ virus (Kos et al., 1986). Later, endogenous circular RNAs processed from pre-mRNAs were identified in both human *Ets-1* (Cocquerelle et al., 1992; Nigro et al., 1991) and mouse *Sry* (Capel et al., 1993) genes. The presence of inverted sequences in flanking introns was suggested to be crucial for mouse *Sry* circularization (Dubin et al., 1995), especially with longer exon circularization (Pasman et al., 1996). However, only a few cases of pre-mRNA processed circular RNAs and their expression levels were reported to be very low, suggesting that they were byproducts of splicing errors (Cocquerelle et al., 1993) and thus likely lacking biological function.

Recently, circular RNAs from human *INK4a/ARF* (Burd et al., 2010) and *CDR1* (Hansen et al., 2013; Hansen et al., 2011) loci were identified and suggested to affect human atherosclerosis risk or regulate mRNA expression, thus shedding new light on physiological roles of circular RNAs. With the advent of high-throughput sequencing from nonpolyadenylated RNA transcripts, thousands of circular RNAs from back-spliced exons were successfully identified in multiple human cell lines (Jeck et al., 2013; Memczak et al., 2013; Salzman et al., 2012, 2013), with suggested function as miRNA sponges (Hansen et al., 2013; Memczak et al., 2013). However, only a few of such circular RNAs contain multiple binding sites to trap one particular miRNA (Jeck and Sharpless, 2014; Guo et al., 2014).

Most circular RNAs from back-spliced exons are stable and cytoplasmic (Jeck et al., 2013; Memczak et al., 2013), possibly due to their resistance to the cellular linear RNA decay machineries. Nevertheless, circular RNA transcripts were generally expressed at low levels compared with linear RNAs (Salzman et al., 2012; 2013). Bioinformatic analyses revealed that back-spliced exons were generally flanked by longer introns, and the existence of *Alu* elements in flanking introns was computationally predicted to be highly associated with the formation of human circular RNAs (Jeck et al., 2013). However, direct experimental evidence and detailed mechanism(s) supporting this model were still lacking.

Here, we take advantage of nonpolyadenylated and RNase R-treated RNA-seq from H9 human embryonic stem cells (hESCs) with a newly developed pipeline to predict back-spliced junctions and systematically characterize circular RNAs. Importantly, we have recapitulated circular RNA formation from a unique expression vector and offer multiple lines of evidence to support the conclusion that circular RNA formation is dependent on flanking complementary sequences, including either repetitive or nonrepetitive elements. Strikingly, such sequences exhibit rapid evolutionary changes among mammals, showing that exon circularization is evolutionarily dynamic. Furthermore, we show that the exon circularization efficiency is regulated by the competition of RNA pairing by complementary sequences within individual introns or across flanking introns. Alternative formation of inverted repeated *Alu* pairs (IR*Alu*s) and the competition between them lead to alternative circularization, resulting

in multiple circular RNA transcripts produced from a single gene.

RESULTS

Computational Pipeline to Precisely Identify Junction Reads from Circularized Exons

Exonic circular RNA is produced from a splice donor site at a downstream exon joining to a splice acceptor site at an upstream exon (back splice). Due to the rearranged exon ordering, specific algorithms are required to annotate these back-spliced exon events for circular RNA prediction. Here, we developed a combined strategy (Figure 1A, CIRCexplorer, Experimental Procedures) to identify junction reads from back-spliced exons. In brief, RNA-seq reads were multiply aligned to the human hg19 reference genome using the TopHat algorithm (Kim et al., 2013) for RNA-seq, and unmapped reads were then uniquely mapped to the human hg19 reference genome with TopHat-Fusion (Kim and Salzberg, 2011) (Figure 1A, step 1). These reads, unmapped with TopHat but mapped with TopHat-Fusion on the same chromosome in a noncolinear ordering (back-spliced ordering), were extracted as candidate back-spliced junction reads. These junction reads were further realigned against existing gene annotation to determine the precise positions of downstream donor and upstream acceptor splice sites, respectively. Due to the sequence similarity at the ends of certain exons, some RNA-seq reads were split at incorrect sites, resulting in mapping to incorrect genomic locations (Figure 1A, red thin bar), usually with a 1–2 nucleotide shift (Figure S1A available online). Such mapping errors were then adjusted with a customized algorithm according to RefSeq exon annotation (Figure 1A, step 2). Finally, exonic circular RNAs were annotated with the support of identified junction reads (Figure 1A, step 3).

We applied this computational strategy to annotate back-spliced junction reads in either poly(A)–/Ribo– (poly(A)–) or RNase R-treated poly(A)– (poly(A)–/RNase R) RNA-seq (Figure S1B) from H9 hESCs. This computational pipeline is highly efficient (Figure S1C), memory economy (Figure S1D), easily accessed, and user friendly due to the application of TopHat (Kim et al., 2013) and TopHat-Fusion (Kim and Salzberg, 2011). It allowed us to detect 2,119 and 9,639 (Figure 1B) exonic circular RNA candidates with at least one back-spliced junction read in poly(A)– (GEO: GSE24399 and GSE60467) or poly(A)–/RNase R (GEO: GSE48003) RNA-seq, respectively (Table S1 for a full list of circular RNAs with at least one junction read). Among them, 1,061 circular RNAs were identified from both samples. On average, their junction reads were about 10-fold enriched after RNase R treatment (Figure 1B, bottom), consistent with previous reports that RNase R treatment is able to enrich circular RNAs from both exonic (Jeck et al., 2013; Salzman et al., 2013; Salzman et al., 2012) or intronic (Zhang et al., 2013) sequences.

To characterize intrinsic features of exon circularization, we next focused in great detail on highly expressed circular RNAs with at least five junction reads from RNase R-treated or untreated poly(A)– RNA-seq samples. Among 1,662 such circular RNAs (Table S2), about 88% of them could also be identified from at least one other cell line (Jeck et al., 2013; Salzman et al., 2013; Memczak et al., 2013), and 12% were predicted only in H9 cells (Figure 1C). Importantly, many of these circular RNAs were confirmed to be processed from back-spliced exons by divergent PCR (Figure S1E and data not shown). In addition, randomly selected circular RNAs (Figures 1D and 1E, left) were further detected by northern blots (NB) on either denaturing PAGE or native agarose gels (Figures 1D and 1E, right). While circular RNAs were resolved on native agarose gels with the same predicted sizes as their linear isoforms, they migrated much more slowly in denaturing PAGE gels, as expected. These RNAs remained stable after RNase R treatment (Suzuki et al., 2006) in both NB (Figures 1D and 1E) and divergent PCR (Figure S1C), further confirming them to be circular.

Alternative Circularization

We identified a number of multiple exon circularization events that were produced from single gene loci. For instance, one region of the human *CAMSAP1* gene produced at least seven distinct exonic circular RNAs from H9 cells, as indicated in Figure 1F, although the majority of these circular RNA isoforms were expressed at low levels. We named this phenomenon alternative circularization (AC). Strikingly, all these AC events and *CAMSAP1* circular RNAs from H9 cells were also predicted from poly(A)–/Ribo– RNA-seq data sets from other ENCODE cell lines (data not shown). In addition, the alternative circularization that leads to multiple circular RNA formation with different expression was observed in many gene loci with different expression levels (Table S1). Together, the existence of alternative circularization suggests yet another layer of gene expression regulation of circular RNA formation.

Circularized Exons Are Preferentially Flanked by Orientation-Opposite *Alu* Elements to Form IR*Alu*s Pairs

Next, we investigated genomic features of highly expressed circular RNAs from Figure 1C. First, the vast majority of highly expressed exonic circular RNAs identified were processed from exons located in the middle of RefSeq genes, with only a few, including the first or the last exons (Figure 2A), suggesting that the circular RNA formation is generally coupled to RNA splicing.

In addition, although 168 out of 1,662 highly expressed circular RNAs contained only one annotated exon, most circular RNAs contain multiple exons, most commonly two to three exons (Figure 2B, left). Interestingly, exons from circular RNAs with only one circularized exon were much longer than those from circular RNAs with multiple circularized exons (Figure 2B, right), indicating that processing may prefer a certain length to maximize exon(s) circularization. Similar genomic features were obtained from highly expressed (junction reads $\geq$ 0.1 RPM) circular RNAs predicted by our pipeline and others (Figures S2A and S2B). Furthermore, flanking introns of circularized exons were much longer (~5-fold) than randomly selected introns (Figure 2C), as reported (Jeck et al., 2013). However, we found that the average *Alu* density in such long flanking introns is comparable to that in other control introns (Figure 2D). This observation thus suggests that longer flanking introns are not necessary for circular RNA formation, but the extended length

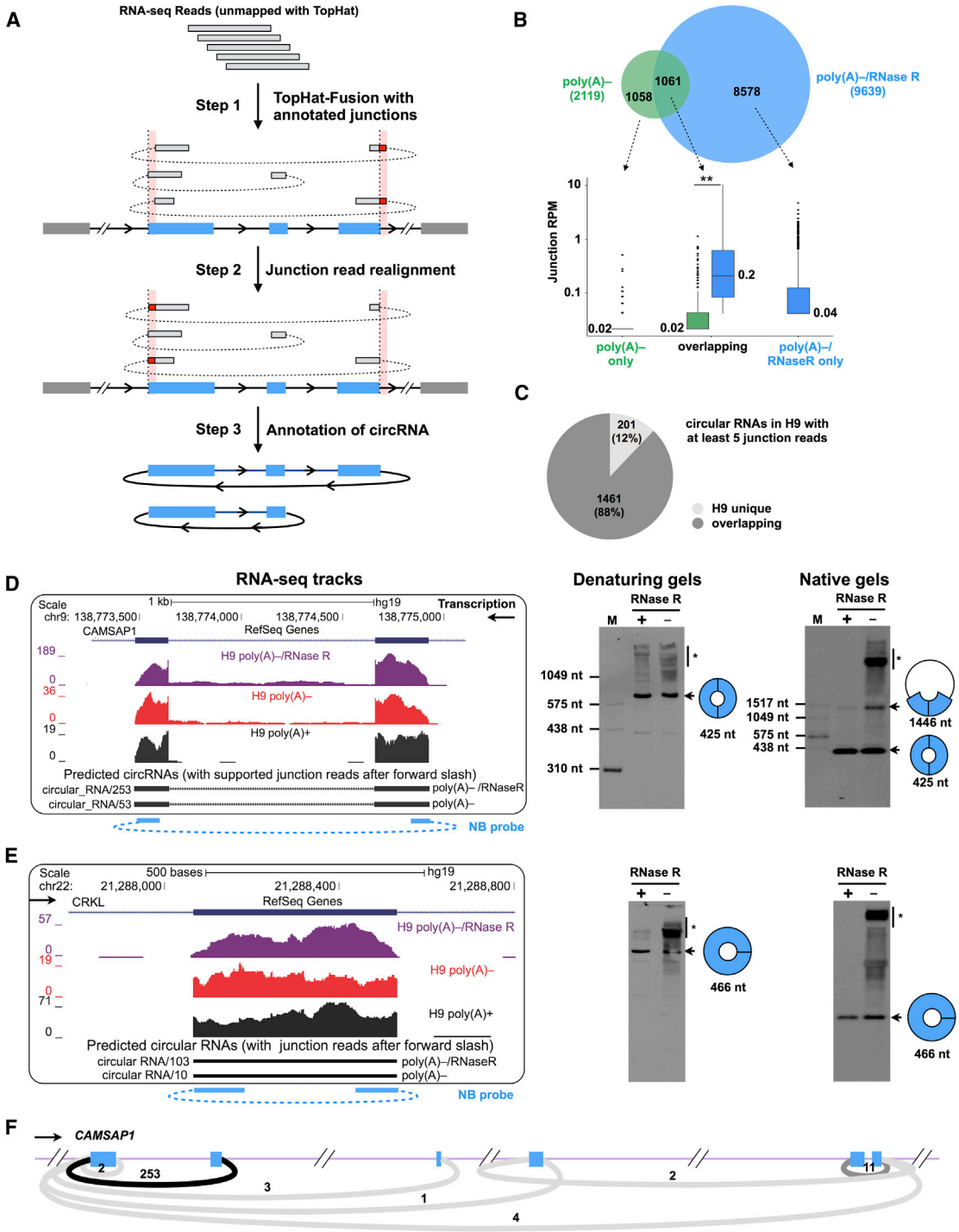

Figure 1. A Customized Algorithm to Determine Exon Circularization and Alternative Circularization

(A) A computational pipeline for back-spliced junction read calling to accurately annotate circular RNAs. The TopHat-Fusion algorithm (Kim and Salzberg, 2011) was first applied to call junction reads (grew thin bars, step 1). Due to sequence similarity at the ends of certain exons (blue bars), mapped junction reads were split (dash arc lines) at incorrect sites, leading to mapping to incorrect locations (red thin bar). Such mapping errors were adjusted with a customized algorithm (step 2). Predicted circular RNAs from back-spliced exons (blue bars) were summed with predicted junction reads (step 3) in Table S1. Exons that do not back splice are indicated as gray bars.

(B) RNase R treatment significantly enriches circular RNA identification. Top, 2,119 or 9,639 (Table S1) events were identified with at least one back-spliced junction read in either poly(A)– RNA-seq (green) or poly(A)–/RNase R treated RNA-seq (blue), respectively. Among them, about 1,061 circular RNAs were

(legend continued on next page)

could introduce more *Alu* elements that, in turn, promote exon circularization.

On average, there were about three *Alu* elements in both upstream and downstream flanking introns of circularized exons (Figures 2E and 2F). Interestingly, *Alu* elements that could form IR*Alu*s, either convergent (Figure 2G) or divergent (Figure 2H), are juxtaposed across flanking introns in a parallel way with similar distances to adjacent exons. In contrast, randomly selected long control intron pairs (at least 10,000 nt in length with no circularized exons identified in H9 cells) have comparable numbers of *Alu*s (Figure S2C); however, the juxtaposition of convergent and divergent IR*Alu*s across them is negligibly correlated (Figure S2D). This thus suggests that IR*Alu*s pairing might bring a splice donor site at a downstream exon and a splice acceptor site at an upstream exon close to each other and promote back splicing. Finally, we also observed that other nonrepetitive complementary sequences were involved in exon circularization, as discussed below.

Circular RNA Formation Is Promoted by IR*Alu*s or by Other Nonrepetitive but Complementary Sequences

Although computational analyses have led to the speculation that IR*Alu*s could promote exon circularization, experimental evidence supporting this model has been lacking. As we have computed that the vast majority of highly expressed circularized exon(s) were found in middle exons of annotated genes (Figure 2A), we cloned the circularized exons along with their full-length flanking introns into the middle of the split e*gfp* gene in pZW1 (Wang et al., 2004). The application of such vectors allowed us to visualize the processed back-spliced exons by NB and linear RNA isoforms by semiquantitative RT-PCR. We selected a representative circular RNA for detailed characterization. This circular RNA contains two exons residing in the human *POLR2A* locus, flanked by relatively short introns with one reverse *Alu* in the upstream intron and two forward *Alu*s in the downstream intron (Figures 3A and 3B). Note that there are two potential pairs of IR*Alu*s formed across flanking introns (red arcs, Figure 3B) with similar predicted free energies (Figure 3B). The endogenous *POLR2A* circular RNA was validated by divergent PCR (Figure S1C) and NB on denaturing PAGE gels in both H9 and HeLa lines (Figure S3A).

For recapitulation, wild-type (Figure 3C, #1) or a series of deletion (Figure 3C, #2–#7) constructs for *POLR2A* circular RNA were individually cloned into pZW1 (Wang et al., 2004). NB validated that recapitulated *POLR2A* circular RNA, with the same migration as endogenous one (Figure S3A), could be produced in clones when flanking IR*Alu*s were formed, including wild-type (Figure 3C, #1) and *Alu* deletions that retained a pair of IR*Alu*s formed across flanking introns (Figure 3C, #3 and #4). In contrast, *POLR2A* circular RNA could not be detected in clones in which deletions eliminated IR*Alu*s pairing across flanking introns (Figure 3C, #2 and #5–#7). It should be noted that the expression of linearized hybrid e*gfp* mRNA (with *POLR2A* exon included) was much higher than that of linearized e*gfp* mRNA (with *POLR2A* exon skipped), as revealed by RT-PCR (Figure 3C), suggesting that exon circularization efficiency is low.

Interestingly, no mouse *POLR2A* circular RNA was identified from RNA-seq (Figure S3B) or divergent PCRs (data not shown) in R1 mouse embryonic stem cells (mESCs). Correspondingly, there are no inverted repeats in the related flanking introns in mouse, providing an explanation for the lack of *POLR2A* circular RNA in mouse. This result indicates the important correlation of inverted repeated complementary sequences (IR*Alu*s in human) with the expression of circular RNAs. Interestingly, human *POLR2A* circular RNA could be also recapitulated when transfected into NIH 3T3 cells in a way that complementary sequences still could promote circular RNA formation (Figure S3C). These results suggest that the machinery for circular RNA formation is evolutionary conserved and that the different organization of inverted repeated complementary sequences between species could lead to different expression levels of circular RNAs.

In addition, *POLR2A* circular RNA could be recapitulated when only a half *Alu* element still remained (Figure 3D, #2 and #3), suggesting that even partially complementary *Alu*s are sufficient to promote RNA pairing (Figure S4A) and exon circularization. Moreover, *POLR2A* circular RNA could also be detected in the reconstituted clone (Figure 3D, #4) in which a pair of IR*Alu*s from the 3′ UTR of the human *NICN1* gene (Chen et al., 2008) (Figure S4B) was inserted into flanking introns to replace the wild-type *POLR2A* IR*Alu*s. Although circular RNAs were expressed at low levels in certain deletions (Figures 3C, #3 and 3D, #3) and replacement (Figure 3D, #4), these results suggest that the formation of this circular RNA is not dependent on specific *Alu* species.

We next hypothesized that any complementary pairing across circularized exons should be able to induce exon

determined before and after RNase R treatment. (Bottom) Box plots of relative expression of predicted circular RNAs from different groups. RNase R treatment significantly enriched circular RNA identification by about 10-fold (**$p < 2.2 \times 10^{-16}$, Wilcoxon rank-sum test). RPM, reads per million mapped reads.

(C) High-confidence circular RNAs from H9 cells (1,662, Table S2) were determined with at least five junction reads from either poly(A)–/RNase R or poly(A)– RNA-seq sample. About 88% (1,461 out of 1,662) of these high-confidence circular RNAs were also identified from six ENCODE cell lines (Salzman et al., 2013). About 12% (201 out of 1,662) were only identified in H9 cells using these accessible data sets.

(D and E) Visualization and validation of two circular RNAs from *CAMSAP1* (D) and *CRKL* (E) loci. (Left) Visualization of predicted circular RNAs. Deep-sequencing signals from poly(A)–/RNase R (purple), poly(A)– (red) or poly(A)+ (black) RNAs were shown. Predicted circular RNAs were indicated with mapped junction reads from either poly(A)– or poly(A)–/RNase R RNA-seq. Northern blot (NB) probes for the circularized exons were highlighted as blue bars. Black arrow indicates the direction of transcription. (Right) RNase R-treated or untreated H9 total RNAs were loaded on a 5% denaturing PAGE gel or on a 1% native agarose gel. NB was performed with probes indicated in left panels. NB bands for circular RNAs are indicated with schematic circles (in blue). Circular RNAs remained stable after RNase R treatment, whereas linear RNAs (asterisk) were removed. Note that a longer *CAMSAP1* circular RNA with an intervening intron between circularized exons was also detected by NB; however, it was unstable by applied RNase R treatment with an unknown mechanism.

(F) A schematic diagram to show alternative circularization in one region of human *CAMSAP1* locus. Circular RNAs with their back-spliced junction reads (numbers) from H9 poly(A)–/RNase R RNA-seq were indicated by arc lines. Different shades of black colors indicated different number of junction reads.

See also Figure S1 and Tables S1 and S2.

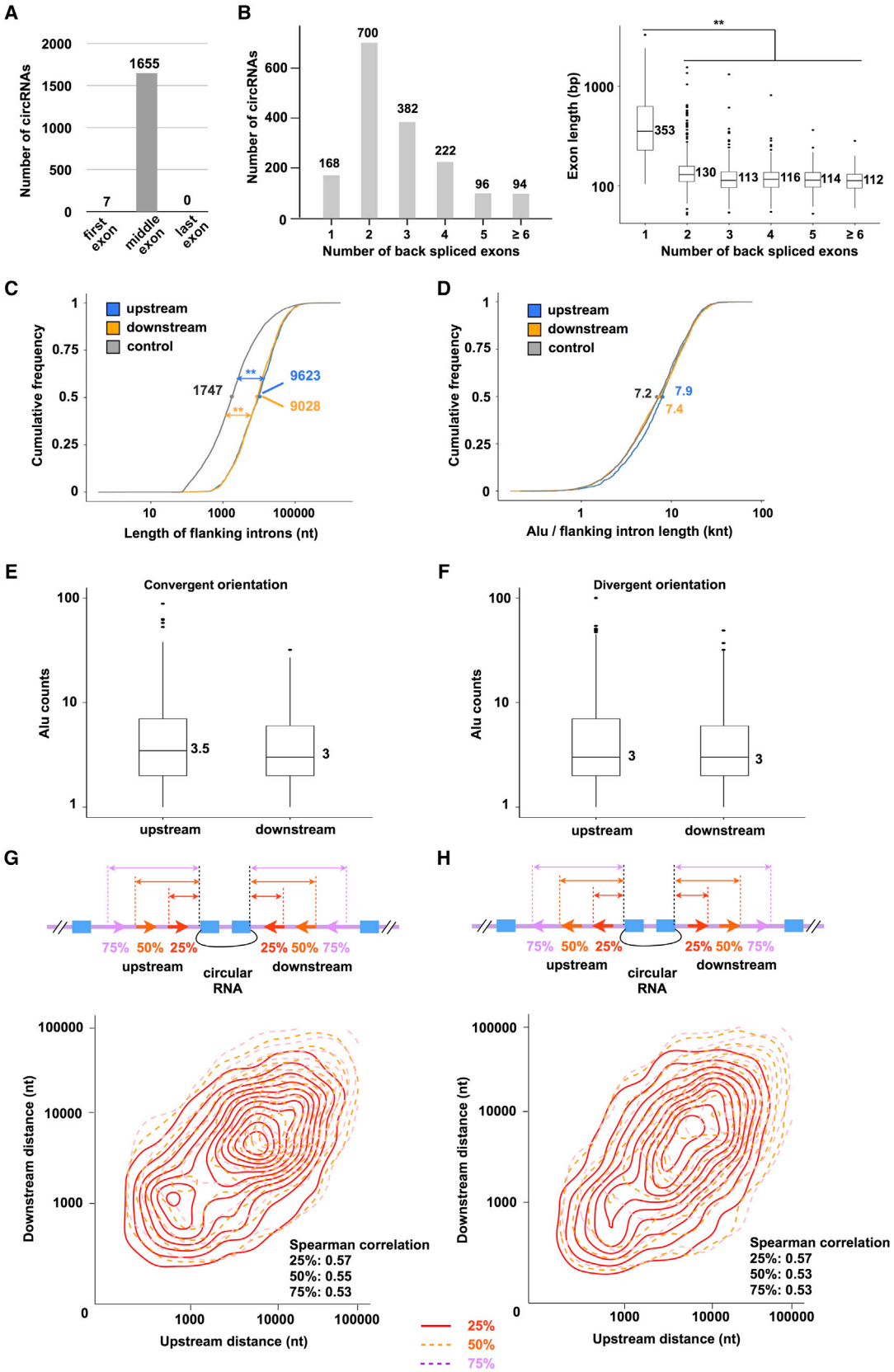

(legend on next page)

circularization. To examine this hypothesis, we further inserted a nonrepetitive fragment from another *POLR2A* intron into both upstream and downstream flanking introns in an orientation-opposite pattern to obtain a new expression vector (Figure 3D, #5). Such insertion allowed the formation of a strong and completely complementary pairing across circularized exons (Figure S4C). Strikingly, *POLR2A* circular RNA expression was much higher in this clone (Figure 3D, #5) than all of the others that we have examined. Correspondingly, in this case, the production of linearized *egfp* mRNA (with *POLR2A* exon skipping for circularization) was comparable with the linearized hybrid *egfp* mRNA (with *POLR2A* exon inclusion), as revealed by RT-PCR (Figure 3D, #5). When this completely complementary structure was disrupted, circular RNA was barely detectable (Figure 3D, #6). Taken together, our results demonstrate that the circular RNA formation is dependent on the pairing capacity of complementary sequences, whether or not they are from repetitive elements.

Naturally Existing Nonrepetitive Complementary Sequences in Flanking Introns Promote Exon Circularization and Undergo Rapid Evolutionary Changes

As we have shown that artificial nonrepetitive complementary sequences can promote circular RNA formation (Figure 3D), it became of interest to identify whether naturally existing nonrepetitive complementary sequences play a role in circular RNA processing. As indicated in Figure 3E, a pair of nonrepetitive complementary sequences (about 180 nt) that naturally exist in the human *GCN1L1* locus was identified with only 3 nt difference (Figures 3E and S5A). As expected, the formation of *GCN1L1* circular RNA was detected by both RNA-seq and RT-PCR in H9 cells (Figure 3E, right).

Intriguingly, these nonrepetitive complementary sequences were largely missing in the mouse *GCN1L1* locus, and circular RNA was undetectable by either RNA-seq or RT-PCR in R1 mESCs (Figure 3E, right). In fact, the endogenous complementary sequences in flanking introns are not only nonconserved between human and mouse, but also undergo rapid changes even among primates (Figures 3F and S5B). These observations suggest that exon circularization may undergo rapid evolutionary changes, shown by *GCN1L1* locus reported here as well as some other gene loci (data not shown).

The Regulation of Circular RNA Formation: Competition of IR*Alu*s Formation across or within Individual Flanking Introns

We have offered new lines of evidence by both computational and experimental analyses to confirm that complementary sequences (mainly IR*Alu*s in the human context) promote circular RNA formation (Figures 2 and 3). However, the existence of IR*Alu*s does not always lead to exon circularization. As indicated in Figure 4A, although multiple *Alu*s and IR*Alu*s across introns could be identified in the human *ZWILCH* locus (left), circular RNA from this locus was undetectable from RNA-seq (middle) or divergent PCR (right) in H9 hESCs. Interestingly, circular RNA in the mouse *ZWILCH* locus was clearly identified from RNA-seq (Figure 4A, middle) and divergent PCR (Figure 4A, right) in R1 mESCs. Thus, what is the mechanism leading to the different expression of *ZWILCH* circular RNA in mouse and human?

Three potential IR*Alu*s within the downstream intron ($IRAlus_{within}$) and another three potential IR*Alu*s across flanking introns ($IRAlus_{across}$) were predicted in the human *ZWILCH* locus (Figure 4B, top). In contrast, the mouse *ZWILCH* region contains three potential inverted complementary SINEs (two pairs of *B1* elements and one pair of *B2* element) within the downstream intron but six potential inverted repeats (*B1* elements) across flanking introns (Figure 4B, bottom). Theoretically, the competition of RNA pairing by complementary sequences across or within individual flanking introns could significantly affect splicing selection and thus exon circularization. With the strong competition for $IRAlus_{within}$ formation, for instance, in the human *ZWILCH* region (Figure 4B, top), splicing occurs at two adjacent exons as a normal constitutive splicing event, which results in a linearized RNA transcript with exon inclusion (Figure S6A), but not exon circularization (Figure 4C, left). In contrast, the predominant formation of $IRAlus_{across}$, such as in the mouse *ZWILCH* region (Figure 4B, bottom), could bring two exons together for back splicing, leading to a linearized RNA transcript with exon skipping (Figure S6B). Such skipped exons undergo circularization to process a circular RNA transcript (Figure 4C, right).

To test this model, we took advantage of the expression construct that expresses *POLR2A* circular RNA at a very high level (#5, Figure 3D) and inserted an additional copy of complementary sequence to introduce potential RNA pairing within the downstream flanking intron (Figure 4D). As expected, because of

Figure 2. Genomic Feature Analyses of Exon Circularization Revealed Juxtaposition of Orientation-Opposite *Alu*s in Flanking Introns

(A) Genomic distribution of back-spliced exons. Most back-spliced exons are located in the middle of genes, and very few of them are the first or the last exons.

(B) Number and length distribution of back-spliced exons. (Left) Most (about 90%) of circular RNAs contain multiple back-spliced exons. (Right) Box plots indicate the distribution of exon length (y axis) from circular RNAs containing different numbers of back-spliced exons (x axis). $^{**}p < 2.2 \times 10^{-16}$, Wilcoxon rank-sum test.

(C) Length distribution of flanking introns. Both upstream (blue line) and downstream (yellow line) flanking introns are much longer than control introns (gray line). $^{**}p < 2.2 \times 10^{-16}$, Wilcoxon rank-sum test.

(D) The density of *Alu* elements in flanking introns. The average *Alu* density in flanking introns (upstream in blue line and downstream in yellow line) is similar to that in randomly selected control introns (gray line).

(E and F) On average, about three *Alu* elements, either convergent (E) or divergent (F), were identified in flanking introns.

(G and H) Juxtaposition of orientation-opposite *Alu* elements in flanking introns. Convergent (G) or divergent (H) *Alu* elements in flanking introns (top) were divided according to their relative positions as first (25%), median (50%) or third quantile (75%). Their relative positions (distances to splice sites) were clustered respectively to create isodenses (curves on which points have the same density) to estimate the overall distribution of *Alu*s in both upstream and downstream flanking introns. Note that IR*Alu*s juxtapose in a parallel manner in introns flanking circular RNA exons with positive correlation (Spearman correlation coefficient > 0.5) (Mukaka, 2012).

See also Figure S2.

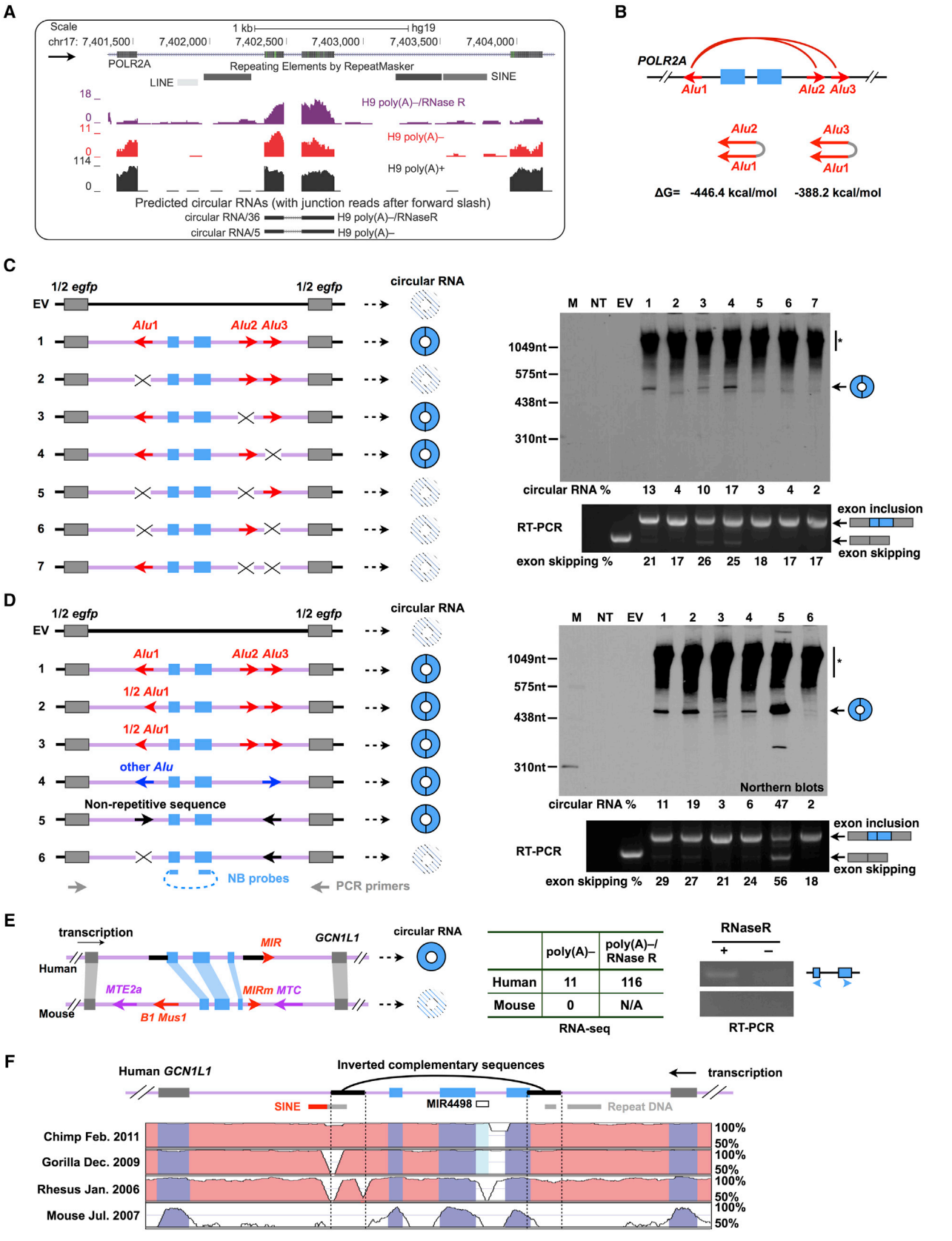

(legend on next page)

the competition of RNA pairing within an individual intron (Figure 4D, left, arc lines), splicing was prone to occur at two adjacent exons as a normal constitutive splicing event, with significantly reduced exon skipping and circularization (#2 and #3, Figure 4D). The reduction of exon skipping was further monitored by RT-PCR (Figure 4D, lower-right). In addition, we found that the expression of recapitulated *POLR2A* circular RNA is positively correlated with that of linear *egfp* mRNA with *POLR2A* exon skipping (Figure 4E). However, to what extent circularization correlates with exon-skipped splicing in endogenous conditions remains to be defined. Taken together, our results strongly indicate that exon circularization can be altered by the competition of RNA pairing within individual introns or across flanking introns and that this alteration can be species specific due to the different distribution of complementary sequences across species (for instance, in *ZWILCH* locus, Figure 4).

The Generality of Exon Circularization with the Competition of IR*Alu*s

We suggest a model that the competition between IR*Alu*s$_{within}$ and IR*Alu*s$_{across}$ alters exon circularization (Figure 4C). To identify the generality of circular RNA formation with the competition of IR*Alu*s$_{within}$ and IR*Alu*s$_{across}$ (Figure 5A), we performed genome-wide comparison of the complementary *Alu* element distribution between the highly expressed circular RNA flanking introns (Table S2) and randomly selected control introns (Figure 2C). Strikingly, the percentage of circular RNA-flanking introns with across-intron IR*Alu*s is 3.49-fold more than that of control introns (Figure 5B, top), suggesting the correlation of complementary sequences with circular RNA formation. Importantly, when competition is counted, the fold is increased to 4.74 (Figure 5B, bottom). In addition, the absolute pair number of (IR*Alu*s$_{across}$ – IR*Alu*s$_{within}$) in circular RNA-flanking introns is much higher than that in control introns (Figure 5C). Together, these genome-wide analyses suggest that the circular RNA formation is generally associated with the competition of IR*Alu*s, but not just IR*Alu*s themselves.

The competition of RNA pairing can be very complicated in endogenous conditions. In addition to the number of potential IR*Alu*s formed across or within flanking introns, the distance between each potential pair of *Alu*s may also affect the pairing capacity. It has been reported that the capacity to form complementary pairs is dramatically decreased when it exceeds several kilobases (Athanasiadis et al., 2004). We found that the distance between the nearest pair of *Alu*s is much longer in randomly selected long control introns (Figure S2C) than that in flanking introns of circularized exons (Figures 5D and 5E). These analyses thus indicate a less probability of RNA pair formation across long control introns. Correspondingly, circular RNAs could not be detected from such control intron regions.

Frequent Alternative Circularization by Widely Distributed *Alu*s in Human Introns

From our computational predictions, we have observed multiple exon circularizations from one gene locus (Figure 1E). In addition to human *CAMSAP1* circular RNAs (Figure 1E), multiple

Figure 3. Recapitulation of Circular RNA Formation with Repetitive or Nonrepetitive Complementary Sequences

(A) An example of identified circular RNA. (Left) Visualization of one predicted circular RNA in human *POLR2A* locus from UCSC genome browser with customized tracks. Annotated SINE (here *Alu*) and LINE elements are located in flanking introns with an orientation-opposite pattern. Predicted circular RNAs with junction read numbers are indicated under wiggle tracks. Black arrow indicated the direction of transcription.

(B) Genomic features of the genomic region for *POLR2A* circular RNA. Back-spliced *POLR2A* exons are indicated as blue bars. Three *Alu* elements in flanking introns are indicated as red arrows to show the polarity. *Alu*1 locates in the upstream intron, and *Alu*2/*Alu*3 locate in the downstream intron. Two potential IR*Alu*s formed across introns are indicated with red arc lines, and their minimum free energies (ΔG) to form RNA pairing are also indicated.

(C) Recapitulation of *POLR2A* circular RNA formation. (Left) A schematic drawing of *egfp* expression vectors with various genomic sequences for *POLR2A* circular RNA recapitulation (#1 to #7). Genomic region for *POLR2A* circular RNA (blue bars) with its wild-type flanking introns (purple lines) was inserted into the pZW1 expression vector (#1). Three *Alu* elements in flanking introns are indicated as red arrows to show the polarity. Half *egfp* sequences from the expression vector backbone are indicated as gray bars. A series of *Alu* deletions are indicated with black crosses (#2 to #7). NB probes for the circularized exons are highlighted as blue bars with dash lines. PCR primers for spliced RNAs are indicated as gray arrows. (Right) Validation of recapitulated circular RNAs by NB and linearized RNAs by RT-PCR. *, linear RNAs.

(D) Nonrepetitive complementary sequences are able to efficiently induce exon circularization. (Left) A schematic drawing of *egfp* expression vectors with wild-type or deletions/replacements of genomic sequences for *POLR2A* circular RNA recapitulation. Either half-*Alu* (#2 and #3), other IR*Alu*s (#4, blue arrows), or nonrepetitive complementary sequences (#5 and #6, black arrows) was tested for exon circularization. (Right) Validation of recapitulated circular RNAs by NB and linearized RNAs by RT-PCR. *, linear RNAs.

(E) Exon circularization at human *GCN1L1* locus with naturally existing nonrepetitive complementary sequences. (Left) A schematic diagram of *GCN1L1* locus for one predicted circular RNA with three back-spliced exons (blue bars). Repetitive elements are indicated with colored arrows in human or mouse. Nonrepetitive complementary sequences were identified in the human, but not in the mouse genome, and are highlighted with black lines. (Right) Junction reads for *GCN1L1* circular RNA were only identified from human H9 cells, but not from mouse R1 cells. The existence of *GCN1L1* circular RNA was confirmed by RT-PCR with divergent primers (blue arrowheads) in human H9, but not in mouse R1 cells.

(F) The naturally existing nonrepetitive complementary sequences undergo rapid evolutionary changes across species. Sequence conservation analysis of *GCN1L1* circular RNA region in different species, visualized with the VISTA browser. (Top) RefSeq exons, including back-spliced (blue bars) and non-back-spliced (gray bars) exons, are indicated. A nonrepetitive complementary sequence (black arrows) was individually identified in both upstream and downstream flanking introns, forming a potential RNA pair highlighted with a black arc line. (Bottom) Rapid evolutionary changes of complementary sequences among primates. y axis, species selected for comparison (left) and levels of conservation based on genomic sequence similarity (right). Colors of conserved regions are labeled by VISTA according to RefSeq annotations (exons in blue shadow and introns in red shadow).

In (C) and (D), equivalent amounts of RNA from cells transfected with each indicated plasmid were resolved on a 5% denaturing PAGE gel for NB to detect circular RNAs. Semiquantitative RT-PCRs further confirmed two isoforms of linearized RNAs. Three biological replicates have been done, and only one set of representative results was shown. The relative abundance of circular RNA and linear RNA with skipped exons was determined by using Quantity One (Bio-Rad). NT, not transfected; EV, empty vector.

See also Figures S3, S4, and S5.

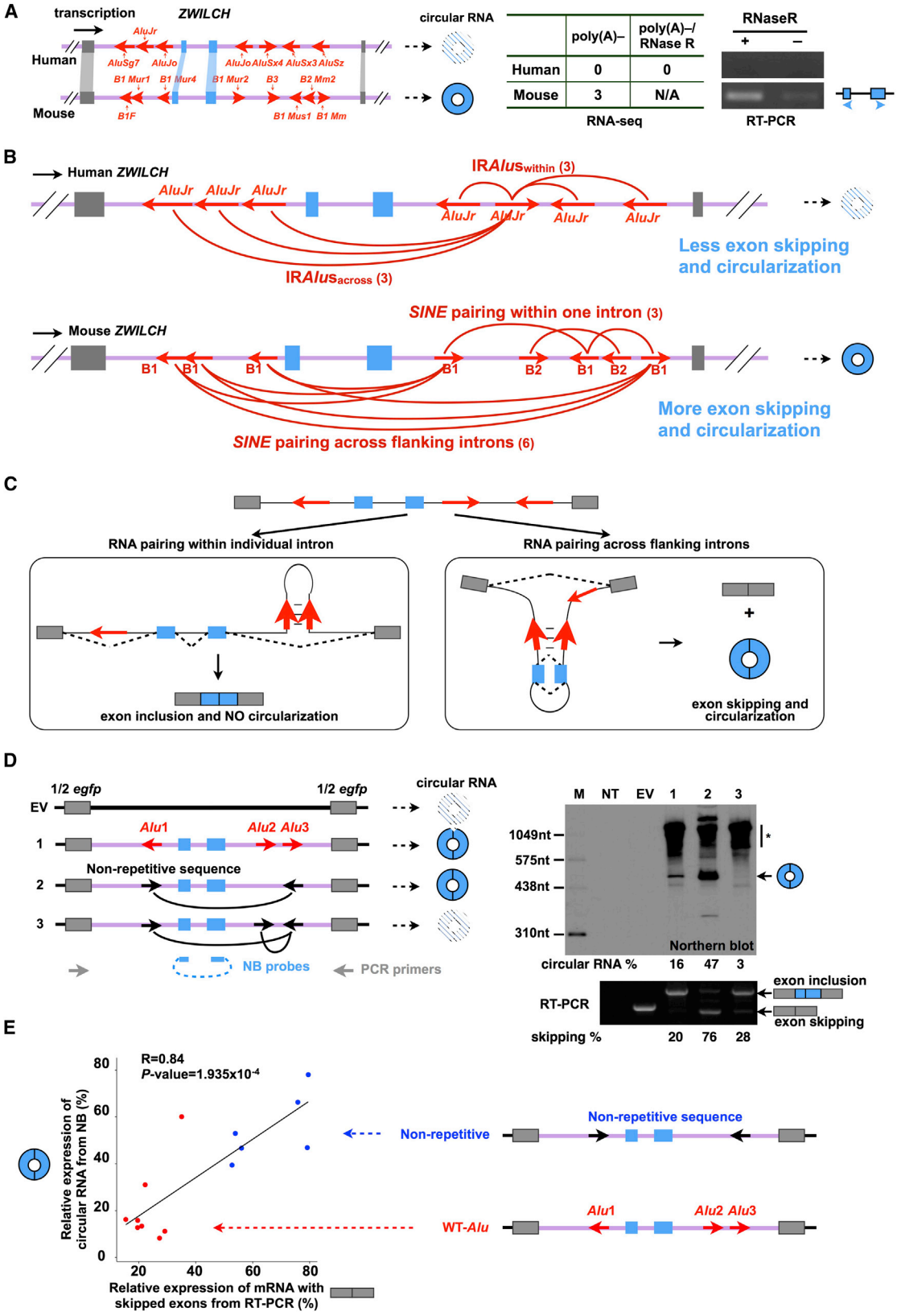

(legend on next page)

DNMT3B (Figure 6A) and *XPO1* (Figure 6B) circular RNAs were also predicted in H9 cells. Importantly, some highly expressed, alternatively circularized *DNMT3B* and *XPO1* RNAs could be separated from NB on denaturing PAGE gels (Figures 6A and 6B), further confirming the existence of alternative circularization as predicted from our computational approach. There are multiple juxtaposed *Alu* elements in *DNMT3B* introns (Figure 6A) and *XPO1* introns (Figure 6B). Computational analyses revealed that these *Alu* elements could form a variety of IR*Alu*s through orientation-opposite patterns (data not shown), which flank alternatively circularized exons (black/gray arcs), suggesting a role of *Alu* pairing and the competition between them in the formation of alternative circularization.

We further confirmed that alternative circularization could be identified from >50% gene loci that produce circular RNAs in examined cell lines (Figures 6C and 6D and Table S1), suggesting the generality of alternative circularization. Frequent alternative circularization might be associated with widely distributed *Alu*s in human introns (Figure 6E). This finding further suggests a previously underappreciated role of intronic *Alu* sequences in the formation of alternative circularization.

DISCUSSION

Due to intrinsic structure features such as lack of 3′ poly(A) tails and no 5′ end caps, genome-wide identification of circular RNAs has been missed in transcriptome profiling from polyadenylated RNAs. Deep sequencing from fractionated nonpolyadenylated RNA populations indicated accumulated signals from certain exons (called excised exons) (Yang et al., 2011), which were further confirmed as circular RNAs (Salzman et al., 2012). These observations were rapidly followed by others who reported numbers of circular RNA transcripts from back-spliced exons from multiple human cell lines after nonpolyadenylated RNA and/or circular RNA enrichment (Jeck et al., 2013; Memczak et al., 2013; Salzman et al., 2012, 2013). However, the mechanism for circular RNA biogenesis and its possible regulation have remained unclear, despite a noted association with *Alu* elements (Jeck et al., 2013).

Here, we developed a computational pipeline to precisely identify back-spliced junction reads for circular RNAs (Figure 1). We characterized circular RNA formation by both bioinformatic (Figure 2) and biochemical (Figure 3) lines of evidence, demonstrating that flanking complementary sequences, including both repetitive and nonrepetitive sequences, play important roles in exon circularization. Interestingly, recapitulation with a pair of perfectly matched complementary sequences led to efficient expression of circular RNAs (Figure 3D), suggesting that the pairing capacity across the circularized exons regulates the productivity of back-spliced circular RNA formation. Strikingly, our data also revealed that naturally existing nonrepetitive complementary sequences are highly associated with exon circularization and undergo rapid evolutionary changes (Figures 3E and 3F). It thus will be of great interest to compare genome wide the formation of circular RNAs and relevant complementary sequences among different species and to further investigate the functional implications of these molecules during evolution. However, we could not exclude the possibility that lack of conservation of some circular RNAs indicates lack of function.

The existence of complementary sequences (either repetitive or nonrepetitive) is necessary, but not sufficient, for exon circularization. The competition of IR*Alu*s formation within individual introns or across flanking introns significantly affects splicing selection and exon circularization (Figure 4), leading to the hypothesis that exon circularization efficiency is altered by the competition of RNA pairing by complementary sequences within individual introns or across flanking introns (Figure 4). It should

Figure 4. The Competition of RNA Pairing by Complementary Sequences Affects Exon Circularization

(A) The presence of IR*Alu*s across flanking introns does not lead to exon circularization. (Left) Detailed genomic organization shows the human (top) or mouse (bottom) *ZWILCH* locus. Repetitive SINE elements are indicated with red arrows. (Middle) No junction read was identified from either poly(A)–/RNase R or poly(A)– RNA-seqs in human H9, and in contrast, at least three junction reads were found in the limited poly(A)– RNA-seq in mouse R1 cells. (Right) The existence of *ZWILCH* circular RNA was further proven by RT-PCR with divergent primers (blue arrowheads) in mouse total RNAs with or without RNase R treatment but was undetected in the human context. N/A, (data) not available.

(B) Potential RNA pairing by IR*Alu*s in the *ZWILCH* locus. Schematic diagrams show the human (top) or mouse (bottom) *ZWILCH* locus with multiple SINE elements (red arrows) in introns flanking a putative circular RNA containing two back-spliced exons (blue bars). Potential inverted repeated *SINE* elements within or across flanking introns are indicated by red arc lines. Note that the same number of IR*Alu*s are predicted either within ($IRAlus_{with}$) or across ($IRAlus_{across}$) flanking introns in the human locus (top), whereas the number of inverted repeated *B1/B2* elements formed across flanking introns is 2-fold higher than that within flanking introns in the mouse homology (bottom).

(C) The competition models of RNA pairing by complementary sequence-mediated exon circularization. (Left) The RNA pairing by IR*Alu*s within one individual intron (red arrows) promotes normal constitutive splicing (dash lines), resulting in a linearized RNA transcript with exon inclusion and no circularization. (Right) RNA pairing by IR*Alu*s across flanking introns promotes back splicing, leading to a linearized RNA transcript with exon skipping and circularization.

(D) Recapitulation assays prove that the competition of RNA pairing by complementary sequences affects exon circularization. (Left) A schematic drawing of *egfp* expression vectors with wild-type (#1) or replacements of genomic sequences for *POLR2A* circular RNA recapitulation. (Right) Equivalent amounts of RNA from cells transfected with each indicated plasmid were resolved on a 5% denaturing PAGE gel for NB to detect recapitulated circular RNAs. RT-PCRs further confirmed two isoforms of linear RNAs. Note that *POLR2A* circular RNA (NB) and linearized *egfp* mRNA with exon skipping (RT-PCR) was dramatically reduced with the competition of RNA pairing (black arc lines) by complementary sequences within one individual intron (#3). Three biological replicates have been done, and only one set of representative results was shown. The relative abundance of circular RNA and linear RNA with skipped exons was determined by using Quantity One (Bio-Rad). NT, not transfected; EV, empty vector. *, linear RNAs.

(E) Positive correlation of recapitulated *POLR2A* circular RNA with linearized *egfp* mRNA. Relative expression of circular RNA (y axis) or linearized *egfp* mRNA with skipped exons (x axis) was individually extracted from NBs or RT-PCRs (Figures 3C, 3D, 4D and S3C and other replicates not shown). Eight biological replicates from results with WT-*Alu* vector and six biological replicates from results with nonrepetitive replacement vector (right) were used for plot (left) to show positive correlation of recapitulated *POLR2A* circular RNA with linearized *egfp* mRNA with exon skipping. $p = 1.935 \times 10^{-4}$, Student's t test.

See also Figure S6.

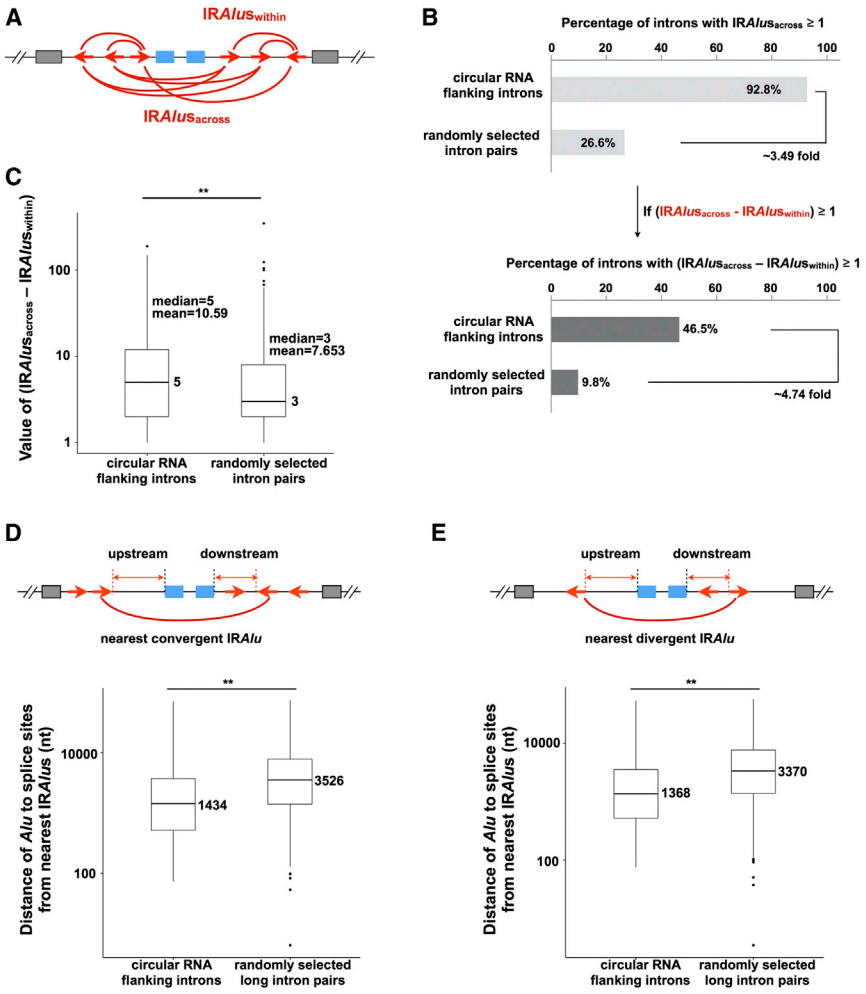

Figure 5. The Generality of Circular RNA Formation with the Competition of IR*Alu*s

(A) Schematic diagram to show the competition of IR*Alu*s$_{across}$ and IR*Alu*s$_{within}$.

(B) IR*Alu*s$_{across}$ are enriched in circular RNA flanking introns and then those in control introns. (Top) The percentage of circular RNA flanking introns with IR*Alu*s$_{across}$ is 3.49-fold higher than that of control introns (compared 92.8% with 26.6%). (Bottom) The percentage of circular RNA flanking introns with (IR*Alu*s$_{across}$ – IR*Alu*s$_{within}$) $\geq$ 1 is 4.74-fold higher than that of control introns (compared 46.5% with 9.8%).

(C) The value of (IR*Alu*s$_{across}$ – IR*Alu*s$_{within}$) in circular RNA flanking introns is much higher than that in control introns. **p = 5.034 × 10^{-12}, Wilcoxon rank-sum test.

(D and E) The distance between the nearest pair of convergent (D) and divergent (E) *Alu*s is much longer in long intron pairs than that in circular RNA flanking introns. **p < 2.2 × 10^{-16}, Wilcoxon rank-sum test.

be noted that the competition of RNA pairing by different distributions of repetitive elements in introns, as well as the circular RNA formation, is evolutionarily dynamic (Figure 4B).

We found that multiple circularized exons could be produced from a single gene locus (Figures 1E, 6A, and 6B), and this phenomenon has also been indicated in some other genes (Burd et al., 2010; Jeck et al., 2013; Salzman et al., 2012). This process is referred to as alternative circularization here to indicate multiple exon circularization selection from a single gene. Because IR*Alu*s forming across flanking introns are strongly associated with exon circularization, we reasoned that the widely distributed *Alu* elements in human introns (Figure 6E) could allow multiple RNA pairing and competitive IR*Alu*s formation to introduce alternative circularization. Accordingly, alternative circularization events were identified in thousands of genomic loci in different cell lines (Figures 6C and 6D). Our findings thus indicate that widespread *Alu* elements in introns and the competition of IR*Alu*s could be actively involved in the selection of alternative circularization in human.

Alternative circularization generates a variety of circular RNAs. In addition to exons only (described here and Jeck et al., 2013; Memczak et al., 2013; Salzman et al., 2012, 2013) or introns only (ciRNAs, Zhang et al., 2013), we found that circular RNAs could be produced from both exons and intron(s) (Figure 1D and Salzman et al., 2012) or from previously unannotated exons (exon x, Figure 6B). Thus, the endogenous conditions for circular RNA formation are very complex. For instance, both the number and the distance between complementary sequences across circularized exons can affect the pairing capability and their competition (Figure 5). Two other mechanisms have also been proposed to indicate circular RNA formation from back-spliced exons, named "direct back-splicing" and "lariat intermediate" (Salzman et al., 2012; Jeck et al., 2013; Jeck and Sharpless, 2014). However, what exactly happens within the circularization-related splicesomes is largely unknown. In addition, the coordination of RNA transcription and exon circularization events also remains elusive. The observation that some circular RNAs are formed by long-range pairing (Figure 6B) suggests that splicing/circularization could occur after transcription despite the cotranscriptional assembly of the spliceosome (Black, 2003). Nevertheless, besides complementary sequences and their competition, it would be interesting to identify other *cis* elements and *trans* factors that are involved in alternative circularization, as has been done in the study of alternative splicing (Fairbrother et al., 2002; Lovci et al., 2013; Nilsen and Graveley, 2010).

The identification of alternative circularization further expands our understanding of gene expression regulation. Through alternative splicing, multiple functional mRNAs (and proteins) could be produced from a single gene (Nilsen and Graveley, 2010). These multiple functional mRNAs are generally thought to exist only as linearized molecules. Our work shows that alternative circularization coupled with alternative splicing can produce a variety of additional circular RNAs from one gene. Taken

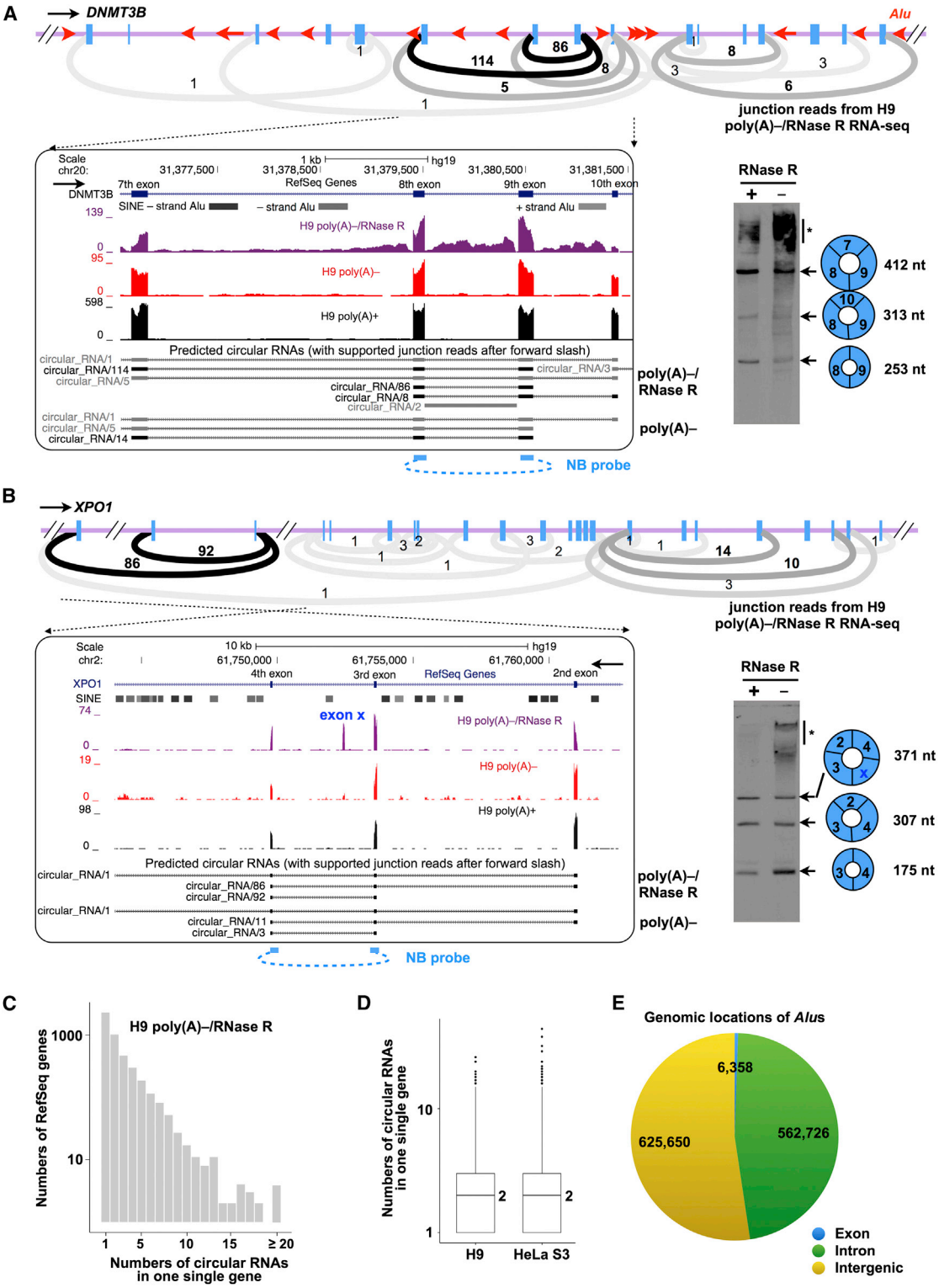

Figure 6. The Diversity of Inverted Repeated *Alu* Pairing and the Competition among Them Lead to Alternative Circularization

(A and B) Alternative circularization leads to a variety of circular RNA transcripts in human *DNMT3B* (A) and *XPO1* (B) loci. (Top) Schematic diagrams to show alternative circularization in one region of examined human loci. *Alu* elements are indicated by red arrows in introns. Circular RNAs with their back-spliced junction reads (numbers) from H9 poly(A)–/RNase R RNA-seq are indicated by arc lines. Different shades of black colors indicated different numbers of junction reads. Note that orientation-opposite *Alu* elements could form potential RNA pairs that flank all of the predicted circular RNAs in *DNMT3B* (A) or *XPO1* (B). (Lower-left)

(legend continued on next page)

together, these lines of evidence imply a new level of complexity in transcriptomes and their regulation.

EXPERIMENTAL PROCEDURES

Additional details can be found in the Extended Experimental Procedures.

Computational Pipeline to Precisely Predict Back-Spliced Junctions for Circular RNAs

We developed a new computational pipeline (CIRCexplorer) by combining TopHat (Kim et al., 2013) and TopHat-Fusion (Kim and Salzberg, 2011) to obtain back-spliced junction reads for circular RNA prediction. See the Extended Experimental Procedures and Figure 1 for details.

Characterization of Back-Spliced Circular RNAs

Information of circularized exons and their flanking introns was extracted from existing gene annotations. Wilcoxon rank-sum test was used for length comparison between exons or introns. Information of repetitive elements was extracted from UCSC RepeatMasker database (rmsk.txt updated at 2009/4/27). Spearman's rank correlation coefficient (Mukaka, 2012) was employed to evaluate the correlation of the juxtaposition of *Alu* elements for divergent or convergent IR*Alu*s. See the Extended Experimental Procedures for details.

Plasmid Construction

For recapitulation of circular RNA, genomic region for *POLR2A* circular RNA with its wild-type flanking introns was amplified and cloned into NheI/MluI-digested pZW1 vector (Zhang et al., 2013). A series of deletions or insertions was further obtained. See the Extended Experimental Procedures for details.

Total RNA Isolation, Polyadenylated/Nonpolyadenylated RNA Separation, RNase R Treatment and RNA-Seq

Total RNA preparation and polyadenylated and nonpolyadenylated RNA separations were carried out as described previously (Yang et al., 2011). RNase R treatment was carried out at 37°C for 3 hr as described previously (Zhang et al., 2013). RNA-seq libraries were prepared by using Illumina TruSeq RNA Sample Prep Kit V2 and were subjected to deep sequencing with Illumina HiSeq 2000 at CAS-MPG Partner Institute for Computational Biology Omics Core, Shanghai, China. See the Extended Experimental Procedures for details.

ACCESSION NUMBERS

Additional raw sequencing data sets and bigWig track files of poly(A)+ and poly(A)–/Ribo– RNA-seq from hESCs H9 and mESCs R1 are available for download from NCBI Gene Expression Omnibus under accession number GSE60467.

SUPPLEMENTAL INFORMATION

Supplemental Information includes Extended Experimental Procedures, six figures, and three tables and can be found with this article online at http://dx.doi.org/10.1016/j.cell.2014.09.001.

AUTHOR CONTRIBUTIONS

L.Y. and L.-L.C. conceived, designed, and supervised the project. X.-O.Z. and L.Y. performed the bioinformatics analysis. H.-B.W., Y.Z., and X.L. performed experiments. L.Y. and L.-L.C. analyzed the data and wrote the paper with input from authors.

ACKNOWLEDGMENTS

We are grateful to Gordon Carmichael for critical reading of the manuscript and Qing-Fei Yin and Hua-Hong Fang for technical support. H9 cells were obtained from the WiCell Research Institute. RNA-seq was performed at CAS-MPG Partner Institute for Computational Biology Omics Core, Shanghai, China. This work was supported by grants XDA01010206 and 2012OHTP08 from CAS; 2014CB964800, 2014CB910600, and 2011CBA01105 from MOST; 31322018 and 31271376 from NSFC; and 2012SSTP01 from SIBS.

Received: July 1, 2014
Revised: August 15, 2014
Accepted: August 27, 2014
Published: September 18, 2014

REFERENCES

Athanasiadis, A., Rich, A., and Maas, S. (2004). Widespread A-to-I RNA editing of *Alu*-containing mRNAs in the human transcriptome. PLoS Biol. *2*, e391.

Black, D.L. (2003). Mechanisms of alternative pre-messenger RNA splicing. Annu. Rev. Biochem. *72*, 291–336.

Burd, C.E., Jeck, W.R., Liu, Y., Sanoff, H.K., Wang, Z., and Sharpless, N.E. (2010). Expression of linear and novel circular forms of an INK4/ARF-associated non-coding RNA correlates with atherosclerosis risk. PLoS Genet. *6*, e1001233.

Capel, B., Swain, A., Nicolis, S., Hacker, A., Walter, M., Koopman, P., Goodfellow, P., and Lovell-Badge, R. (1993). Circular transcripts of the testis-determining gene Sry in adult mouse testis. Cell *73*, 1019–1030.

Chen, L.L., and Carmichael, G.G. (2008). Gene regulation by SINES and inosines: biological consequences of A-to-I editing of Alu element inverted repeats. Cell Cycle *7*, 3294–3301.

Chen, L.L., DeCerbo, J.N., and Carmichael, G.G. (2008). Alu element-mediated gene silencing. EMBO J. *27*, 1694–1705.

Cocquerelle, C., Daubersies, P., Majérus, M.A., Kerckaert, J.P., and Bailleul, B. (1992). Splicing with inverted order of exons occurs proximal to large introns. EMBO J. *11*, 1095–1098.

Cocquerelle, C., Mascrez, B., Hétuin, D., and Bailleul, B. (1993). Mis-splicing yields circular RNA molecules. FASEB J. *7*, 155–160.

Dubin, R.A., Kazmi, M.A., and Ostrer, H. (1995). Inverted repeats are necessary for circularization of the mouse testis Sry transcript. Gene *167*, 245–248.

Fairbrother, W.G., Yeh, R.F., Sharp, P.A., and Burge, C.B. (2002). Predictive identification of exonic splicing enhancers in human genes. Science *297*, 1007–1013.

Visualization of predicted circular RNA in human *DNMT3B* (A) and *XPO1* (B) loci from UCSC genome browser with customized tracks. Predicted circular RNAs with junction read numbers are indicated under wiggle tracks. Black arrows indicate the direction of transcription. Note that many more *Alu* elements are annotated in *XPO1* (B) than those in the *DNMT3B* (A) locus; thus more complicated alternative circularization was also observed in the *XPO1* (B) locus. (Lower-right) RNase R-treated or untreated H9 total RNAs were loaded on a 5% denaturing PAGE gel for NB. Circular RNAs remained stable after RNase R treatment, whereas linear RNAs (asterisk) were largely diminished. Multiple circular RNAs were clearly resolved by NB. Numbers in schematic diagram of circular RNAs (lower-right) were indicated as annotated RefGene exon orders (lower-left). Note that a novel exon (exon x) was identified in *XPO1* (B) circular RNA(s) after RNase R treatment. *, linear RNAs.

(C) Distribution of RefSeq genes (y axis) with different numbers of circular RNAs (x axis). About half of RefSeq genes that generate circular RNAs are able to produce multiple circular RNAs with at least one back-spliced junction read from hESCs H9 poly(A)–/RNase R and/or poly(A)– RNA-seq data set.

(D) Box plots indicate the distribution of circular RNA numbers (y axis) in one single RefSeq gene. Note that, on average, two circular RNAs could be determined from one single gene in both hESCs H9 poly(A)–/RNase R RNA-seq and ENCODE HeLa S3 poly(A)– RNA-seq (GEO: GSE26284).

(E) Distribution of *Alu* elements in human genome. Among >1.1 million *Alu* elements in human genome (Chen and Carmichael, 2008), about half of them are located in intron regions.

Guo, J.U., Agarwal, V., Guo, H., and Bartel, D.P. (2014). Expanded identification and characterization of mammalian circular RNAs. Genome Biol. *15*, 409.

Hansen, T.B., Wiklund, E.D., Bramsen, J.B., Villadsen, S.B., Statham, A.L., Clark, S.J., and Kjems, J. (2011). miRNA-dependent gene silencing involving Ago2-mediated cleavage of a circular antisense RNA. EMBO J. *30*, 4414–4422.

Hansen, T.B., Jensen, T.I., Clausen, B.H., Bramsen, J.B., Finsen, B., Damgaard, C.K., and Kjems, J. (2013). Natural RNA circles function as efficient microRNA sponges. Nature *495*, 384–388.

Jeck, W.R., and Sharpless, N.E. (2014). Detecting and characterizing circular RNAs. Nat. Biotechnol. *32*, 453–461.

Jeck, W.R., Sorrentino, J.A., Wang, K., Slevin, M.K., Burd, C.E., Liu, J., Marzluff, W.F., and Sharpless, N.E. (2013). Circular RNAs are abundant, conserved, and associated with ALU repeats. RNA *19*, 141–157.

Kim, D., and Salzberg, S.L. (2011). TopHat-Fusion: an algorithm for discovery of novel fusion transcripts. Genome Biol. *12*, R72.

Kim, D., Pertea, G., Trapnell, C., Pimentel, H., Kelley, R., and Salzberg, S.L. (2013). TopHat2: accurate alignment of transcriptomes in the presence of insertions, deletions and gene fusions. Genome Biol. *14*, R36.

Kos, A., Dijkema, R., Arnberg, A.C., van der Meide, P.H., and Schellekens, H. (1986). The hepatitis delta (delta) virus possesses a circular RNA. Nature *323*, 558–560.

Lovci, M.T., Ghanem, D., Marr, H., Arnold, J., Gee, S., Parra, M., Liang, T.Y., Stark, T.J., Gehman, L.T., Hoon, S., et al. (2013). Rbfox proteins regulate alternative mRNA splicing through evolutionarily conserved RNA bridges. Nat. Struct. Mol. Biol. *20*, 1434–1442.

Memczak, S., Jens, M., Elefsinioti, A., Torti, F., Krueger, J., Rybak, A., Maier, L., Mackowiak, S.D., Gregersen, L.H., Munschauer, M., et al. (2013). Circular RNAs are a large class of animal RNAs with regulatory potency. Nature *495*, 333–338.

Mukaka, M.M. (2012). Statistics corner: A guide to appropriate use of correlation coefficient in medical research. Malawi Med. J. *24*, 69–71.

Nigro, J.M., Cho, K.R., Fearon, E.R., Kern, S.E., Ruppert, J.M., Oliner, J.D., Kinzler, K.W., and Vogelstein, B. (1991). Scrambled exons. Cell *64*, 607–613.

Nilsen, T.W., and Graveley, B.R. (2010). Expansion of the eukaryotic proteome by alternative splicing. Nature *463*, 457–463.

Pasman, Z., Been, M.D., and Garcia-Blanco, M.A. (1996). Exon circularization in mammalian nuclear extracts. RNA *2*, 603–610.

Salzman, J., Gawad, C., Wang, P.L., Lacayo, N., and Brown, P.O. (2012). Circular RNAs are the predominant transcript isoform from hundreds of human genes in diverse cell types. PLoS ONE *7*, e30733.

Salzman, J., Chen, R.E., Olsen, M.N., Wang, P.L., and Brown, P.O. (2013). Cell-type specific features of circular RNA expression. PLoS Genet. *9*, e1003777.

Sanger, H.L., Klotz, G., Riesner, D., Gross, H.J., and Kleinschmidt, A.K. (1976). Viroids are single-stranded covalently closed circular RNA molecules existing as highly base-paired rod-like structures. Proc. Natl. Acad. Sci. USA *73*, 3852–3856.

Suzuki, H., Zuo, Y., Wang, J., Zhang, M.Q., Malhotra, A., and Mayeda, A. (2006). Characterization of RNase R-digested cellular RNA source that consists of lariat and circular RNAs from pre-mRNA splicing. Nucleic Acids Res. *34*, e63. http://dx.doi.org/10.1093/nar/gkl151.

Wang, Z., Rolish, M.E., Yeo, G., Tung, V., Mawson, M., and Burge, C.B. (2004). Systematic identification and analysis of exonic splicing silencers. Cell *119*, 831–845.

Yang, L., Duff, M.O., Graveley, B.R., Carmichael, G.G., and Chen, L.L. (2011). Genomewide characterization of non-polyadenylated RNAs. Genome Biol. *12*, R16.

Zhang, Y., Zhang, X.O., Chen, T., Xiang, J.F., Yin, Q.F., Xing, Y.H., Zhu, S., Yang, L., and Chen, L.L. (2013). Circular intronic long noncoding RNAs. Mol. Cell *51*, 792–806.